Nano-size effects in graphite/graphene structure exposed to cesium vapor

Cite as: J. Appl. Phys. **124**, 123304 (2018); https://doi.org/10.1063/1.5037028
Submitted: 20 April 2018 . Accepted: 04 September 2018 . Published Online: 28 September 2018

A. S. Mustafaev, V. I. Yarygin, V. S. Soukhomlinov, A. B. Tsyganov, and I. D. Kaganovich

Nano-size effects in graphite/graphene structure exposed to cesium vapor

A. S. Mustafaev,[1] V. I. Yarygin,[2] V. S. Soukhomlinov,[1,3] A. B. Tsyganov,[3] and I. D. Kaganovich[4]
[1]*Department of General and Technical Physics, Saint-Petersburg Mining University, Saint-Petersburg, Russia*
[2]*Institute for Physics and Power Engineering, Obninsk, Russia*
[3]*Department of Optics, Saint-Petersburg State University, Saint-Petersburg, Russia*
[4]*Princeton Plasma Physics Laboratory, Princeton, New Jersey 08543, USA*

(Received 20 April 2018; accepted 4 September 2018; published online 28 September 2018)

A thermionic energy converter with a nickel collector and cesium vapor as a working gas was studied, and an abnormally low value of the surface work function of ≈1 eV was obtained if the collector was covered by a thin carbon layer. Scanning electron microscopy x-ray microanalysis data of the elemental composition of the collector's surface after its long exposure to plasma indicate that the carbon structure was intercalated with cesium atoms, and this change to surface structure can be a reason for the anomalously low work function ∼1 eV. The thermionic energy converter with such a collector demonstrated high heat-to-electric power conversion efficiency up to ∼20%. *Published by AIP Publishing.* https://doi.org/10.1063/1.5037028

I. INTRODUCTION

Composite carbon nanostructures with a low work function are of considerable interest for numerous applications ranging from electron emission devices[1–3] to ion-battery technologies.[4] It is known that adding hydrogen atoms or alkali metals to the surface of carbon structures can lead to remarkable reduction of the surface work function.[5–10] These surface effects can be used in thermionic energy converters (TICs) of the thermal power into electric. The TIC can also be used for solar energy conversion technologies and on-board nuclear power supply systems for space vehicles.[11–16] Because of surface effects enhancing operation of TIC, efficiency of nuclear powered TIC can be increased multiple times and life time an order of magnitude up to 10% and 1 year, respectively, for example, for TOPAZ International program.[14]

It is well known that the voltage generated by the TIC is mostly determined by the difference of the work functions of the emitter and collector. It is difficult to increase the work function of the emitter by choosing the appropriate material for the emitter, because the emitter has to produce sufficient current at a given temperature. Therefore, the only way to increase efficiency is to reduce work function of the collector.

Previously, Ref. 17 reported that TIC high efficiency for conversion of the thermal into electrical power was achieved, if the cesium vapor was introduced through a perforated collector into the TIC inter-electrode gap. Cesium was continuously introduced into the TIC through the collector and then condensed on the walls of the vacuum chamber, into which the TIC was installed. The collector has a large number of small diameter (0.07 mm) holes (1000 holes per cm^2). The collector's surface (outside of the holes) was preliminary covered with a thin layer of the finely dispersed carbon with a thickness of about 0.1 mm. According to Refs. 18–20, a necessary condition to achieve high efficiency for conversion of the TIC is a preliminary activation of the electrodes for at least one hour with the following parameters: the emitter temperature, $T_E = 1570$ K, the collector temperature, $T_C = 670$ K, and the cesium reservoir temperature, $T_{Cs} = 570$–670 K.

We performed an independent study of similarly prepared TIC but introduced some improvements.[21–23] We compared TIC operation in a standard configuration where Cs was introduced into inter-electrode gap from a side and in the enhanced regime where cesium vapor was flowing through the collector holes. The thermionic energy converter with such a collector demonstrated high heat-to-electric power conversion efficiency up to ∼20% at $T_E = 1570$ K and $T_C = 670$ K. The achieved high efficiency of the TIC makes small nuclear power electric stations economically viable.

The goal of this study is to perform an analysis of surface modifications of the collector after long exposure to Cs vapor and to develop a physics model explaining the achieved anomalously low work function.

II. VOLT-AMPERE CHARACTERISTICS OF THE TIC AND COLLECTOR WORK FUNCTION

TIC had a variable inter-electrode gap ($d = 0.2$–3 mm) into which cesium vapor was introduced either through sides (standard mode) or through collector holes. The emitter was made from the polycrystalline Mo pellet and has 14 mm diameter and is 11 mm thick; a thin layer (3 μm) of Pt was deposited on emitter. The collector was an 8 mm diameter thin (0.2 mm thick) Ni disc. The collector's surface outside the holes was covered by carbon micro-flakes, which were produced by applying the aqueous carbon water solution and subsequent drying. In the central part of the collector (4×4 mm), 121 holes of 0.07 mm diameter were drilled by a pulsed laser.[22,23]

The emitter was heated by an electron beam. The measurement of the electrodes temperature was performed by five tungsten-rhenium micro thermocouples as well as an optical micropyrometer. The remaining impurities pressure was 10^{-8} Torr without Cs vapor and 10^{-6} Torr when Cs vapor was introduced into the TIC. The Cs pressure was determined

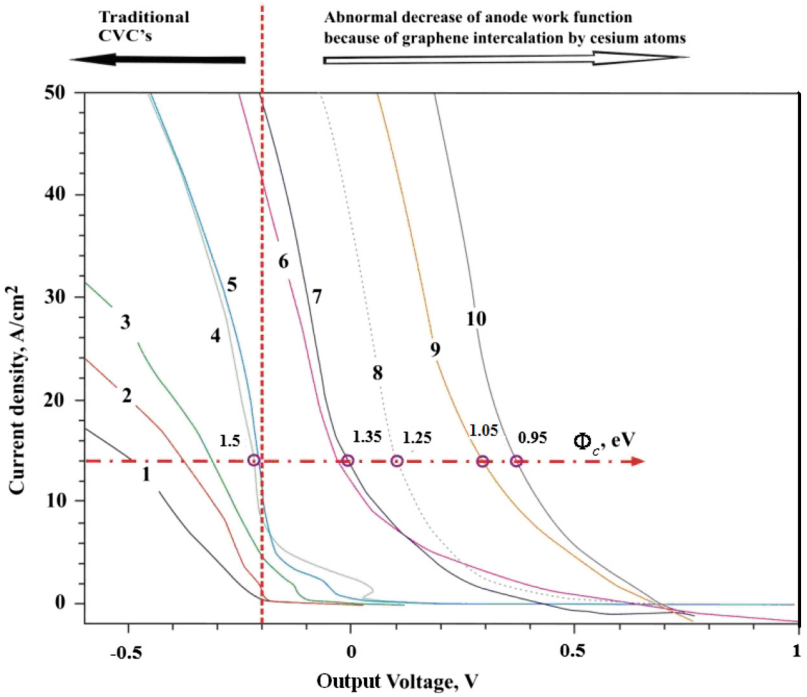

FIG. 1. The TIC current-voltage characteristics. T_E = 1350 K, T_C = 750 K, T_{Cs} = 570 K, d = 0.3 mm. The curves correspond to the activation time in minutes: 1–0; 2–6; 3–17; 4–32; 5–65; 6–160; 7–165; 8–180; 9–185, 10–190.

as saturated Cs vapor pressure at the temperature of the liquid cesium source.

The converter's current voltage characteristics (CVCs) were measured by scanning the output voltage by a DC power driver, starting from the stationary current-voltage point, corresponding, as a rule, to the standard mode of the TIC operation with a minimal current. After optimization of the current-voltage characteristics in standard Cs vapor mode, the activation of the TIC electrodes by flow of Cs through collector holes was performed, as proposed in Refs. 22 and 23. TIC was operated for long time ~1000 hours, during which time transition from one mode operation to another was repeated several dozen times.

The CVC varies depending on the duration passed after electrode activation by the Cs flow through the collector holes. An example of CVC measurements is shown in Fig. 1. Analysis of the output electrical characteristics of the TIC showed that the vacuum work function of the emitter was Φ_{E0} = 5–5.15 eV. This is typical for a polycrystalline Mo covered with Pt. Also, vacuum work function of the emitter Φ_{E0} was practically independent of the collector temperature in the range T_C = 650–1000 K.

Curves 6–10 in Fig. 1 correspond to effective energy generation by the TIC. These curves show a dramatic decrease of the collector work function after about 2 hours since its activation. The collector work function was measured making use of "the return current method" using Richardson-Dashman equation for thermionic emission, see method details in Refs. 24–26

$$j_s = A_0(1-R)T_C^2 \exp\left(-\frac{\Phi_c}{kT_C}\right), \quad (1)$$

where $A_0 = 4\pi mek^2h^{-3}$ is the Richardson's constant, R is the electron reflection coefficient, Φ_C is the work function of the collector, m is the electron mass, e is elementary charge, k is the Boltzmann constant, and h is the Planck constant.

Curve 10 demonstrates that the collector work function decreases down to the anomalous value of 0.95 eV; the obtained result is unique.

Figure 2 shows the measured work function of the TIC, Φ_C, using "the emission method" (see method details in Refs. 24–26) for T_E = 1300 K as a function of ratio of temperature of collector to that of the reservoir of cesium for different operation methods of the TIC. Curve 1 corresponds to the TIC operating in the standard mode, when Cs is supplied from the sides. Cs pressure is determined as pressure of

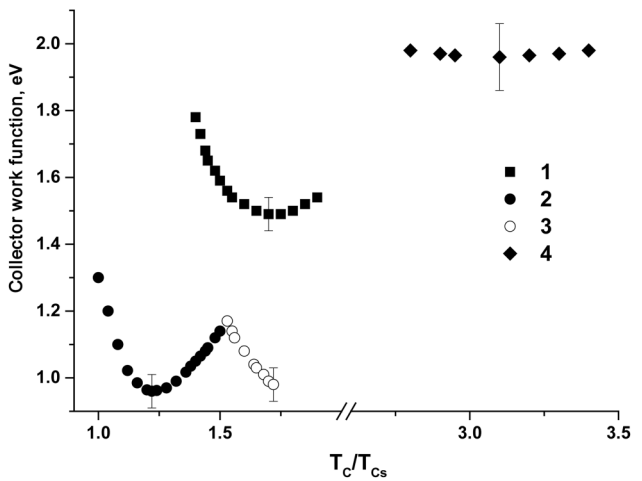

FIG. 2. The work function of the TIC for T_E = 1300 K as a function of ratio of temperature of collector to that of the reservoir of cesium after activation process: 1—TIC operates in the standard mode, when Cs is supplied from the sides; 2—electrode activation by Cs flows through collector holes; 3—standard mode during 25 hours after electrode activation by flow of Cs through collector holes; 4—standard mode but practically without Cs, the collector temperature varied in the range 800–1000 K.

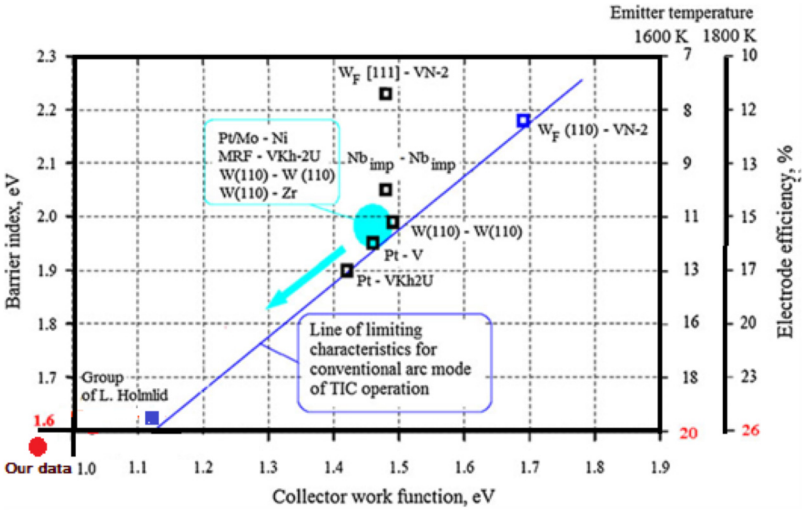

FIG. 3. Barrier Index and device efficiency is a function of collector work function for different emitters and emitter temperatures.

saturated vapor corresponding to temperature of the liquid Cs reservoir. From Fig. 2, it is evident that the measured work function of the TIC is higher than (1.5 ± 0.05) eV for $T_C/T_{Cs} = (1.75 \pm 0.10)$. When electrodes are activated by Cs flow through the holes (curve 2), the work function is anomalously low: (0.95 ± 0.05) eV for $T_C/T_{Cs} = (1.25 \pm 0.10)$. It is well known that energy efficiency of TIC most depends on the so-called barrier index—sum of the Φ_C and the volume losses of energy for the plasma creation φ_C (which cannot be really adjusted in TIC construction). Achieved value of collector work function $\Phi_C = 0.95$ eV and $\varphi_C = 0.64$ eV[22,23] corresponds to Barrier index of 1.59 eV. As can be seen from Fig. 3,[22,23] the TIC estimated efficiency rate is more than 20%.

After 25 hours of operation in this regime, the TIC regime was switched back to the standard mode with Cs supply from the reservoir (curve 3). From Fig. 2, it is evident that the measured work function of the TIC remained low (0.95 ± 0.05) eV, but for much higher values of $Tc/T_{Cs} = (1.75 \pm 0.10)$. Comparison of curves 1 and 3 shows that not Cs presence in plasma is responsible for the anomalously low work function, but it is rather due to activation of the collector. We also performed measurements of Φ_C by two independent methods, both without Cs plasma present. For the first measurements, the temperature of the Cs reservoir was reduced to 300 K and Cs was practically absent ($P_{Cs} \approx 10^{-4}$ Torr and $d = 0.3$ mm) for $T_E = 1300$ K, T_C varied in the range 800–1000 K. Obtained by using "the emission method" value of $\Phi_c = (1.95 \pm 0.10)$ eV and is shown by curve 4. The second method used photoelectron method and obtained value of $\Phi_c = (2.00 \pm 0.05)$ eV. Measurement was performed at the Princeton Institute for the Science and technology of Materials (PRISM).

We performed surface analysis of the TIC collector, which, as described above, consists of the nickel substrate covered with carbon flakes and exposed for a long time, during ~1000 hours of TIC operation with cesium. *In situ* characterization of collector is difficult because the TIC collector operates at high temperatures ~700 K and high cesium vapor pressures (in the range of 1–10 Torr). For this reason, after the cesium vapor was pumped out, and collector was cooled down, the collector was removed from TIC under vacuum and analyzed with a scanning electron microscope (Merlin by Carl Zeiss) with an energy dispersive x-ray detector (X-Max by Oxford Instruments) with the goal to obtain the composition of chemical elements at the surface layer of the collector.

III. SCANNING ELECTRON MICROSCOPY X-RAY MICROANALYSIS DATA OF THE COLLECTOR'S SURFACE

Figure 4 shows the Scanning Electron Microscopy (SEM) image of the surface of the collector (20 keV beam energy, image was obtained in the secondary electron collection mode). Note the formation of the dark concentric rings around the holes in the collector.

To explain the nature of the dark concentric rings, SEM-images were obtained with a higher resolution both in the ring and outside. Figure 5 shows the zoom-in SEM-image of the collector surface in the region between the dark rings; the images show an irregular structure of the dispersed carbon micro-flakes formed after application of

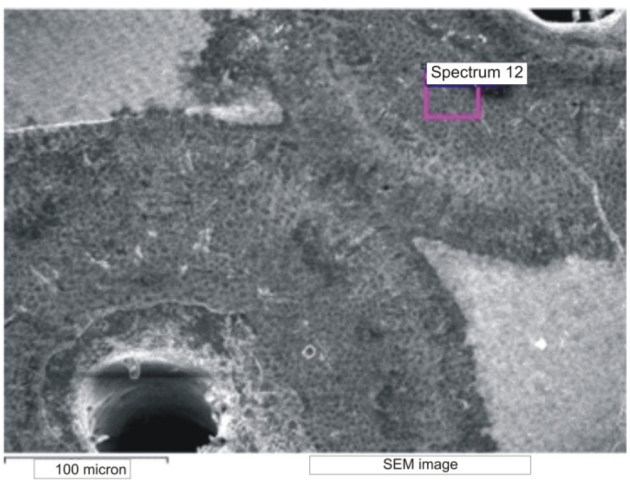

FIG. 4. SEM image of the collector's surface (secondary electron detection mode) using 20 keV beam.

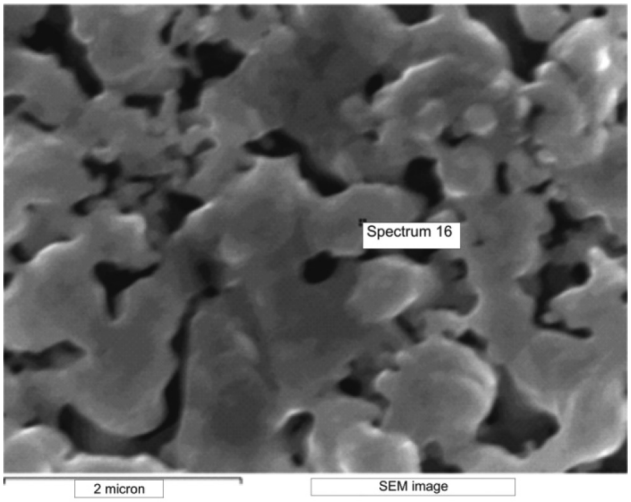

FIG. 5. SEM image of the collector's surface outside of the dark concentric rings zones.

aqueous graphite suspension. This structure of carbon micro-flakes did not change even after the long exposure (~1000 hours) to plasma during operation of the TIC. Figure 6 shows x-ray spectrum and composition of chemical elements derived from the x-ray spectrum in the point on the surface of a carbon flake, marked "16," obtained by sample exposure to fast electrons of the microscope beam and was detected using an Oxford Instruments detector. Numerical simulation of the fast electron trajectories in the sample was performed using Monte Carlo method with the help of CASINO code (Prof. Raynald Gauvin, Université de Sherbrooke, Québec, Canada, http://www.gel.usherbrooke.ca/casino/What.html) in order to determine the size of the zone from which the x-rays radiation occurs. As a result, it was concluded that the depth of the x-ray zone on the collector's surface was about 0.9 microns.

From the spectrum shown in Fig. 6, it is evident that, outside the dark concentric rings, the collector's surface layer to the depth of up to 0.9 microns contains a significant amount of carbon atoms originating from graphite and contains some amount of oxygen atoms. The carbon layer is sufficiently thick so that the electron beam does not reach the nickel surface of the substrate. Therefore, the "apparent" Ni atoms concentration is low. A significant amount of Mo atoms, which were transferred to the collector by evaporating from the emitter, are also present in the spectrum. In contrast, the Pt atoms are not detected on the surface of the collector, though platinum was initially applied to the emitter surface. This is due to the fact that platinum may not be subjected to evaporation under given conditions, because it remains alloyed with the emitter material at the surface. It is especially necessary to note the absence of any signal from Cs atoms in Fig. 6.

However, SEM-image structure changed dramatically for the dark concentric rings (Fig. 7). Instead of overlapping carbon flakes of irregular form, grains with sufficiently rectilinear boundary appeared, and their average size increased significantly as compared to flakes. The transformation of initially overlapping carbon micro-flakes into uniform grains of a similar thickness with regular boundaries occurs, probably, due to effects of Cs vapor flowing through the holes at sufficiently high collector temperature (~750 K). The transformation process of initially irregular carbon micro-flakes into regular grains appears to start at the boundaries of the holes in the collector and then gradually spreads radially over the collector's surface.

Figure 8 shows the x-ray spectrum of the region designated as "Spectrum 21" in Fig. 7. Note the appearance of an appreciable amount of Cs atoms, which are absent in the areas outside of the concentric rings (e.g., x-ray spectrum in Fig. 6). This can be explained by the fact that before removing the collector from the TIC chamber for *ex situ* analysis, the container with cesium was cooled to a room temperature and cesium was pumped out. In the region outside of the concentric rings in Fig. 4, the Cs atoms being only physically adsorbed on the surface of the carbon flakes and hence were pumped out. In contrast, in the region within the dark concentric rings in Fig. 4, Cs atoms diffused and intercalated into the space between the graphene sheets constituting the modified carbon grains and therefore could not be pumped out.

The observed increase in the proportion of O atoms according to the x-ray spectrum in Fig. 8 is probably due to oxidation of cesium. The relative decrease in the proportion of Ni atoms is due to increased thickness of carbon grains intercalated by Cs atoms, which screen the underlying nickel

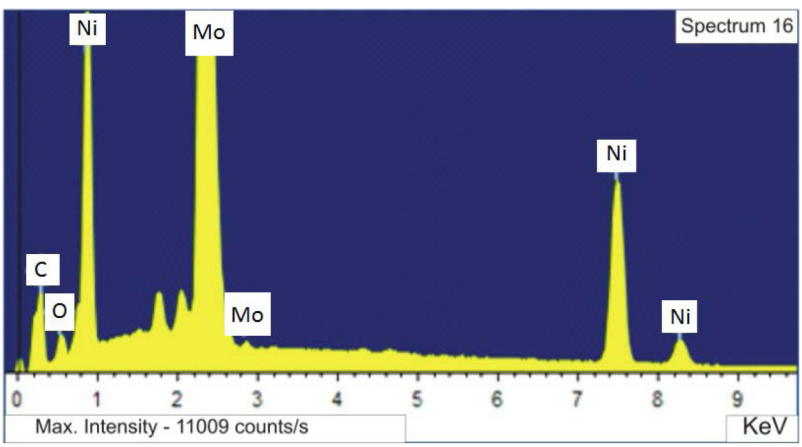

FIG. 6. X-ray spectrum of the region marked "Spectrum 16" in Fig. 2. The ratio of atomic concentrations of the elements C:O:Ni:Mo:Cs is 47%:5%:27%:21%:0%.

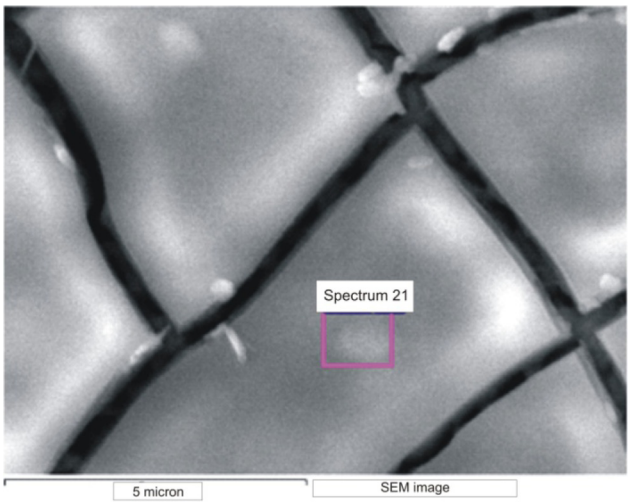

FIG. 7. SEM image of the surface structure of the collector in the region of concentric rings around the holes.

substrate. The relative portion of Mo atoms decreased, probably because Mo atoms are loosely bound to the outer graphene layers of the modified carbon grains.

IV. PHYSICS MODEL OF MODIFIED COLLECTOR SURFACE RESPONSIBLE FOR LOW WORK FUNCTION

The efficient reduction of the work function of the sample collector to about 1 eV can be explained due to formation of the modified carbon grains formed from graphene layers intercalated with Cs atoms on the surface of the nickel collector.

In the standard operation regime of TIC, Cs atoms absorb at the surface of the collector. This is well-known to yield reduction of the work function to about 1.5 eV (see curve 1 in Fig. 2).

During Cs flow through the collector holes, oxygen absorb on its surface (possibly from remaining impurities, which pressure is about 10^{-8}–10^{-6} Torr and wall out gassing). Estimates show that a monolayer of oxygen can form with second-minutes depending on remaining pressure. As shown in Ref. 27, oxygen molecules dissociate on graphene defects. Defects on graphene surface may also allow Cs atoms to penetrate in between carbon layers and bond with oxygen atoms on the surface of graphene. A possible resulting atomic structure of the surface is shown in Fig. 9(b). Here, O atoms are covalently bound to a Cs atom, which are intercalated under the topmost graphene monolayer of the modified carbon grain. Cs atoms originate from the cesium vapor flowing inside the holes. A second layer of top most Cs atoms originates from cesium vapor absorbing on the collector surface. These Cs atoms are also bound to O atoms, forming Cs-O-Cs structures. Note that this structure formed at the collector surface is very similar to the structure of an Ag-O-Cs photocathode, which is also known to have the lowest electron work function known, of the order of 1 eV.

The structure shown in Fig. 9(b) may explain the reason for low work function as follows. Molecules of oxides of rare earth elements have a high value of the electric dipole moment. For example, for LaO, HfO, and ZrO the dipole electric moment value is in the range of 0.6–0.8 eA. Similarly, dipole moment of CsO is 0.6 eA. Because of the presence of CsO electric dipoles on the surface, the whole structure work function is reduced, similar to other surfaces with electric dipoles.[28] In our case of carbon with the work function 4.5 eV, dipoles have to reduce the work function by 3.5 eV. As shown in Refs. 28 and 29 to achieve such reduction of the work function, the surface density of dipoles should be $\mu \approx 0.02$e/A. Assuming that Cs atoms are placed in the middle of carbon sextuples with area 8.76 A^2 (Ref. 30) and the CsO electric dipole momentum is 0.6 eA gives the surface density of dipoles $0.6\,\text{eA}/8.76\text{A}^2 = 0.07$ e/A. Therefore, for observed reduction of the work function the surface density of Cs-O molecules should be $\theta_c = \frac{0.02}{0.07} \approx 0.3$. Note if $\theta_c => 1$ neighboring electric dipoles start affecting each other by tilting and then mean electric field of the resulting structure may reduce and affect the work function. Possibly, this can explain minimum of the work function as a function of parameter T_C/T_{Cs}, which controls the surface density of Cs–O molecules.

For the standard mode of TIC operation, the collector surface is heated to $T_C > 900$ K and then the topmost layer of Cs atoms is desorbed, see Fig. 9(c), and correspondingly the work function is increased from 0.95 eV to about 2 eV. If the Cs reservoir temperature is low ($T_{Cs} = 300$ K), Cs vapor

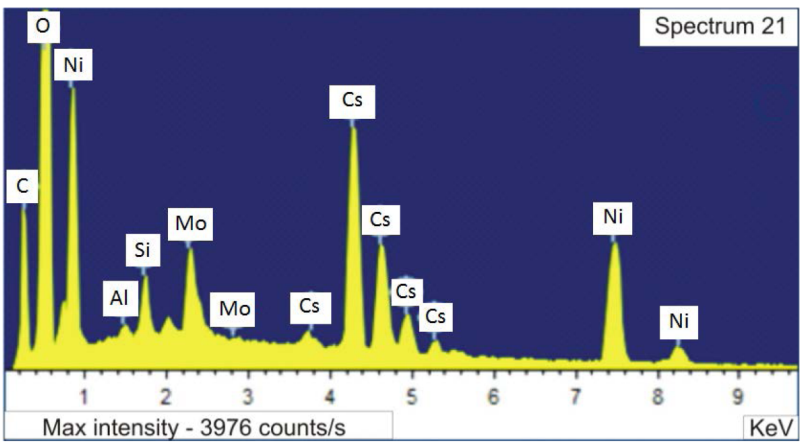

FIG. 8. X-ray spectrum of the region shown in Fig. 7. Ratio of atomic concentrations of the elements C:O:Ni:Mo:Cs is 27%:53%:12%:2%:10%.

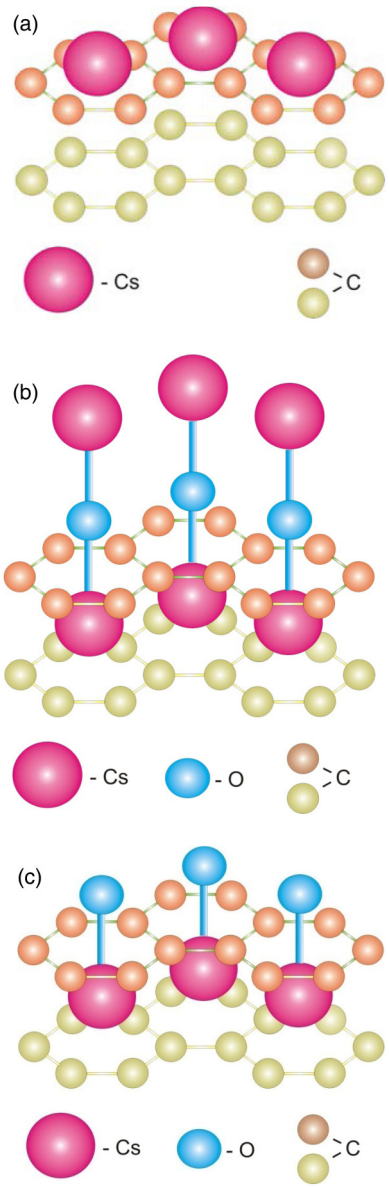

FIG. 9. (a) Atomic structure of the collector for the conditions corresponding to curve 1 in Fig. 2. (b) Atomic structure of the collector for the conditions corresponding to curves 2 and 3 in Fig. 2. (c) Atomic structure of the collector for the conditions corresponding to curve 4 in Fig. 2 (the collector surface is heated to $T_C > 900$ K, and the Cs reservoir temperature is low $T_{Cs} = 300$ K).

pressure is very low and there is no sufficient Cs condensation on the surface to replenish top layer.

As can be seen from Figs. 6 and 8, the relative amount of oxygen on them does not correspond to the model described above. These data were indeed obtained after the sample was moved from the vacuum chamber and exposed to the air, as suggested by the Referee. Also, some amount of the water molecules (hydrogen atoms are not seen in x-ray spectra) may additionally penetrate due to absorption into the film and increase O atoms signal in x-ray. Therefore, the oxygen signal does not correspond to the sample at operational conditions of TIC. However, the observed signal supports the proposed hypothesis of graphene layers intercalated by Cs atoms in the following way. Oxygen molecules dissociate on the graphite surfaces.[31] Moreover, it is well-known that if alkali metals are deposited on the surface of the graphite, the desorption temperature of atmospheric gases increases dramatically.[32] Therefore, the increased x-ray signal from oxygen supports our hypothesis of graphene layers intercalated by Cs atoms, because the presence of cesium increases the adsorption energy of oxygen atoms. Correspondingly, the amount of absorbed oxygen in the area of dark concentric ring zones is much higher than outside of these zones.

As discussed above, the SEM x-ray microanalysis measured integrated signal from ~1 micron depth of the sample. Boundaries of the regular rectangular grains are very long, tens of micrometers and the cracks between boundaries reach depth of the entire carbon film up to the nickel substrate (see Fig. 7). Correspondingly, oxygen atoms can penetrate deep into cracks and intercalate many layers of graphene. This process is not possible for the carbon films outside the area of dark concentric ring zones, because the carbon flakes in that area do not have such deep long crack to allow for oxygen (and cesium) to penetrate graphite.

Regarding the SEM x-ray measurements of molybdenum atoms being different for different samples, this difference can be probably explained by difference of adsorption energy of molybdenum atoms to different surfaces. Molybdenum atoms evaporated from overheated (~1500 K) emitter are impinging on the carbon film. We suppose that for the carbon film in the form of non-structured irregular flakes shown in Fig. 5, the Mo atoms may adsorb on the carbon surface and can considerably contribute to the x-ray signal. However, in the case of carbon film in the form of modified regular grains shown in Fig. 7, Mo atoms are not adsorbed on the carbon surface of these grains, and therefore the x-ray signal is weaker.

V. CONCLUSIONS

We propose a physical model of the observed anomalously low electron work function of the TIC collector due to formation of a structure on its surface. This low electron work function explains the high efficiency of thermal emission converters with such a collector. During a prolonged exposure to cesium vapor at a pressure of 1–10 Torr and a temperature of about 750 K, the dispersed carbon flakes of a thickness of about 0.5 micron and size of about 3 micrometers in diameter initially randomly deposited on the surface of the perforated nickel collector in the areas surrounding the holes in the collector are transformed into rectangular carbon grains with a size of about 5–10 micrometers with straight regular boundaries and identical thickness. Such carbon grains consist of graphene layers intercalated with Cs atoms. It is proposed that on the top most grapheme layer of the transformed carbon grain, a structure is formed, where Cs-O molecules are positioned on top of the graphene layer and in the middle positions of carbon sextuple in graphene, whereas other cesium atoms intercalate in between the graphene sheets. Such a surface structure has a low work function (<1 eV), similar to the well-known photocathode Ag-O-Cs,

and explains the anomalous reduction of the collector work function and corresponding increase in the TIC efficiency.

Further studies of the surface properties of the effective collectors in thermionic energy converters are necessary; however, standard methods of *in situ* surface analysis are not applicable under conditions of cesium vapor and high surface temperature.

ACKNOWLEDGMENTS

The authors would like to thank Professor V. Polischuk from ITMO University for his valuable technical support on SEM measurement, Yao-Wen Yeh for technical assistance in measurements of the work function at PRISM, and Dr. Yevgeny Raitses for valuable discussions. Igor Kaganovich would like to acknowledge the Office of Science, Department of Energy, Basic Energy Sciences, Materials Sciences and Engineering Division, for supporting the measurements of the work function at PRISM and his effort.

[1]J. D. Rameau, J. Smedley, E. M. Muller, T. E. Kidd, and P. D. Johnson, Phys. Rev. Lett. **106**, 137602 (2011).
[2]X. Chang, Q. Wu, I. Ben-Zvi, A. Burrill, J. Kewisch, T. Rao, J. Smedley, E. Wang, E. M. Muller, R. Busby, and D. Dimitrov, Phys. Rev. Lett. **105**, 164801 (2010).
[3]K. Tada and K. Watanabe, Phys. Rev. Lett. **88**, 127601 (2002).
[4]C. Casas and W. Li, "A review of application of carbon nanotubes for lithium ion battery anode material," J. Power Sources **208**, 74–85 (2012).
[5]W. Pickett, Phys. Rev. Lett. **73**, 1664 (1994).
[6]A. Tiwari, EuroPhys. Lett. **108**, 46005 (2014).
[7]D. P. Bernatskii and V. G. Pavlov, Tech. Phys., **58**(6), 809–813 (2013).
[8]V. Robinson, T. S. Fisher, J. A. Michel, and C. M. Lukehart, Appl. Phys. Lett. **87**, 061501 (2005).
[9]D. Bernatskiiet and V. G. Pavlov, Tech. Phys. **58**, 809 (2013).
[10]H. Yuan, S. Chang, I. Bargatin, N. C. Wang, D. C. Riley, H. Wang, J. W. Schwede, J. Provine, E. Pop, Z.-X. Shen, P. A. Pianetta, N. A. Melosh, and R. T. Howe, Nano Lett. **15**, 6475 (2015).
[11]H. Yuana, D. C. Riley, Z.-X. Shen, P. A. P. Nicholas A, M. R., and T. Howe, Nano Energy **32**, 67 (2017).
[12]J. W. Schwede, I. Bargatin, D. C. Riley, B. E. Hardin, S. J. Rosenthal, Yun Sun, F. Schmitt, P. Pianetta, R. T. Howe, Z.-X. Shen, and N. A. Melosh, Nat. Mater. **9**, 762 (2010).
[13]S. Adams, AIP Conf. Proc. **813**, 590 (2006).
[14]National Research Council Committee on Thermionic Research and Technology. *Thermionics Quo Vadis? An Assessment of the DTRA's Advanced Thermionics Research and Development Program* (National Academy, Washington, DC, 2001), pp. 1–70.
[15]G. P. Smestad, Sol. Energy Mater. Sol. Cells **82**, 227–240 (2004).
[16]A. Sommer, J. Appl. Phys. **51**, 1254 (1980).
[17]L. Holmlid and R. Svenson, U.S. patent 5578886A (26 November 1996).
[18]L. Holmlid, in *Proceedings of Thermionic Energy Conversion Specialist Conference*, *Göteborg* (University of Göteborg, 1993), p. 47.
[19]R. Svensson, L. Holmlid, and E. Kennel, in *Proceedings of Thermionic Energy Conversion Specialist Conference*, *Göteborg* (University of Göteborg, 1993), p. 93.
[20]R. Svensson, and L. Holmlid, in *Proceedings of 32nd Intersociety Energy Conversion Engineering Conference* (American Nuclear Society, 1997), p. 1071.
[21]V. I. Yarygin, V. N. Sidel'nikov, and I. I. Krasikov, JETP Lett. **77**, 330 (2003).
[22]V. Yarygin, J. Cluster Sci. **23**, 77 (2012).
[23]V. I. Yarygin and A. S. Mustafaev, Russ. J. Phys. Chem. **B9**, 546 (2015).
[24]G.N. Hatsopoulos and E.P. Gyftopoulos, *Thermionic Energy Conversion* (MITPress, 1973), Vol. 1.
[25]F. G. Baksht, G. A. Dyuzhev *et al*., *Thermionic converters and low-temperature plasma*. English Edition edited by Lorin K. Hansen. (Technical Information Center/ US DoE, 1978), 484 pp. ISBN-10: 0870793012. ISBN-13: 978-0870793011.
[26]V. I. Yarygin, V. A. Ruzhnikov, and V. V. Sinyavskiy, *Space and Land-Based Nuclear Energy Conversion Devices* (NIYaU, MIFI, 2016) (in Russian).
[27]X. Qi, X. Guo, and C. Zheng, Appl. Surf. Sci. **259**, 195 (2012).
[28]R. D. Suenram, F. J. Lovas, G. T. Fraser, and K. Matsumura, J. Chem. Phys. **92**, 4724 (1990).
[29]V. Vlahos, J. H. Booske, and D. Morgan, Appl. Phys. Lett. **91**, 144102 (2007).
[30]L. Pauling, J. Am. Chem. Soc. **49**, 765 (1927).
[31]R. T. Yang and C. Wong, J. Chem. Phys. **75**, 4471 (1981).
[32]H. P. Bonzel, Surf. Sci. Rep. **8**, 43–125 (1987).